

1 **From Surface processes to Marine Ice-Sheet Instability: The Collapse of the Barents–**
2 **Kara Ice Sheet during the last deglaciation**

3 **V. van Aalderen^{1,2,3}, S. Charbit^{1,2}, A. Quiquet^{1,2} and C. Dumas^{1,2}**

4 ¹Laboratoire des Sciences du Climat et de l'Environnement (LSCE), CEA, CNRS, UVSQ, Université
5 Paris-Saclay, Gif-sur-Yvette, France

6 ²Institut Pierre-Simon Laplace (IPSL), Université Versailles Saint-Quentin, Guyancourt, France

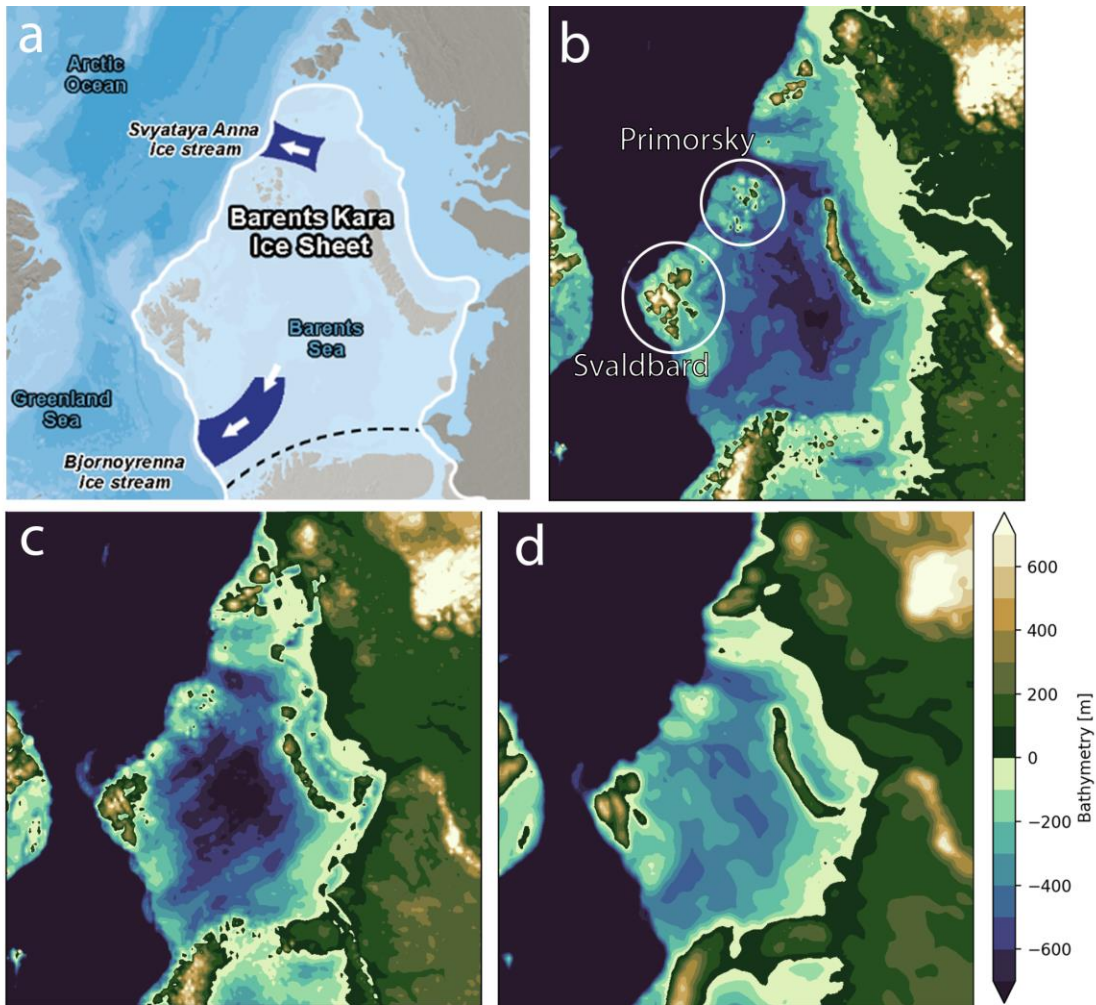
7 ³Institut des Géosciences de l'Environnement (IGE), Université Grenoble Alpes, CNRS, IRD, INRAE,
8 Grenoble INP, Grenoble, France.

9 Corresponding author: Victor van Aalderen (victor.van-aalderen@univ-grenoble-alpes.fr)

10

11 Supplement

12 1. Figures



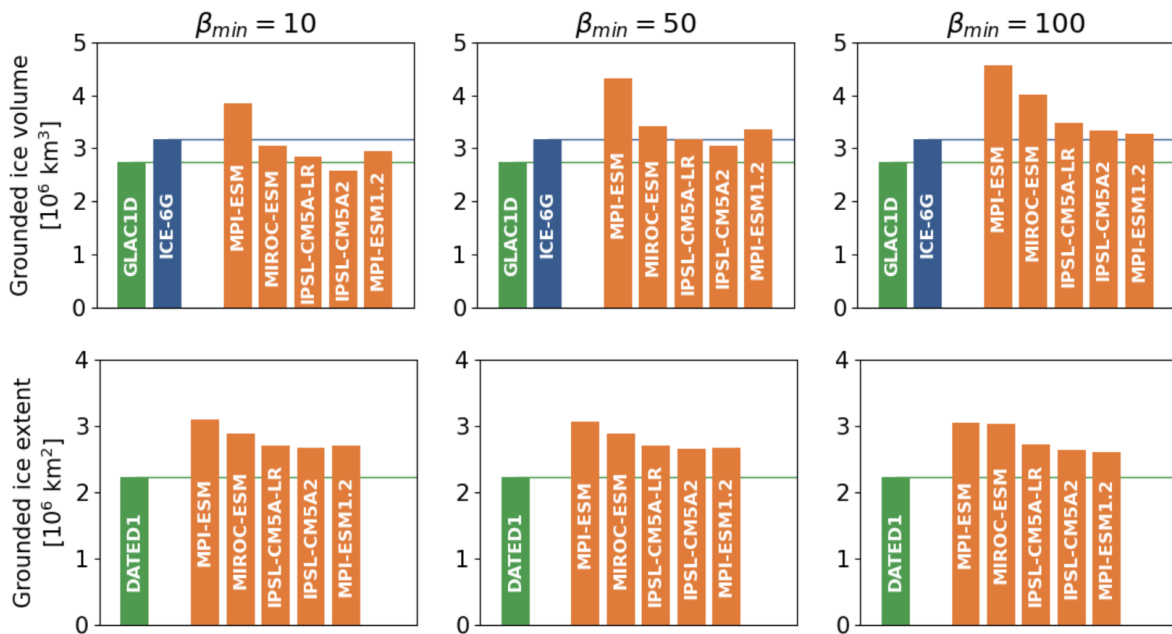
13
14 **Figure S1:** a: Map of the Barents-Kara ice sheet at the LGM. The white line is the most credible ice extent
15 of the Eurasian ice sheet at the LGM according to the DATED-1 compilation (Hughes et al., 2016). Dark
16 blue areas correspond to the location of the main ice streams (Dowdeswell et al., 2016; Stokes and Clark,
17 2001), and dotted black lines are delimitations between the Fennoscandian and the Barents-Kara ice
18 sheets. b: Topography of BKIS at the LGM according to the DEGLA-MPI-iLOVECLIM-10 simulations. Blue
19 areas are below the LGM sea level, while brown/green areas are above the LGM sea level. c. same as b,
20 but for the ICE-6G_C reconstruction. d. same as b, but for the GLAC1D reconstruction. For both c and d, the
21 LGM topography was calculated by computing the topographic anomaly between the LGM and the pre-
22 industrial period from the respective reconstructions and adding it to present-day observations to achieve
23 a higher spatial resolution.

24
25
26

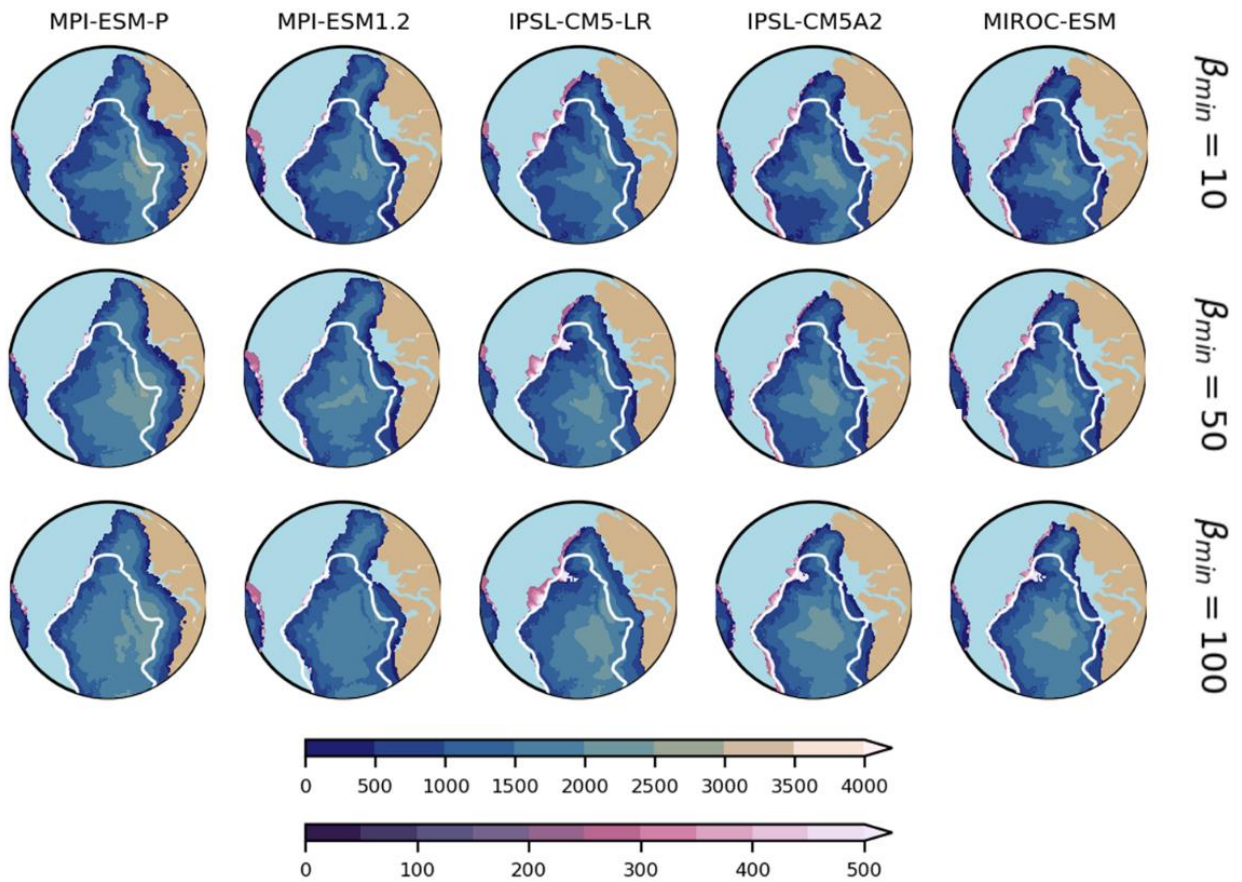
27 We performed 15 equilibrium simulations by using the LGM climate simulated with 5 different
 28 PMIP3/PMIP4 experiments to generate ice sheets in good agreement with geological
 29 reconstructions. To explore the impact of basal stress we ran simulations with three different
 30 values for the minimum basal friction, setting β_{min} to 10, 50, or 100 Pa.s.m⁻¹.

31
 32 Figure S2 shows the total volume of the BKIS ice sheet at the end of the 100,000-year simulations
 33 for different GCM forcins abd different β_{min} values. Our results indicate that higher β_{min} values
 34 lead to an overestimation of ice volume compared to the GLAC1D and ICE-6G_C reconstructions
 35 (Add references here for both reconstructions). A lower basal friction allows ice streams to flow
 36 more rapidly, making it more difficult to sustain thick ice upstream, as ice is transported away
 37 more efficiently. Consequently, simulations with $\beta_{min} = 10$ Pa.s.m⁻¹ produce lower ice volumes
 38 that better match with reconstructions compared to higher β_{min} values.

39
 40 However, β_{min} has no significant influence on the simulated ice sheet extent (see Figs. S2 and
 41 S3). This can be explained by the fact that the northern boundaries of BKIS are constrained by
 42 the edge of the continental shelf, making it difficult for ice to form in deeper waters, and by
 43 temperatures above the melting point in the continental part of BKIS (Siberia and Northern
 44 Europe).

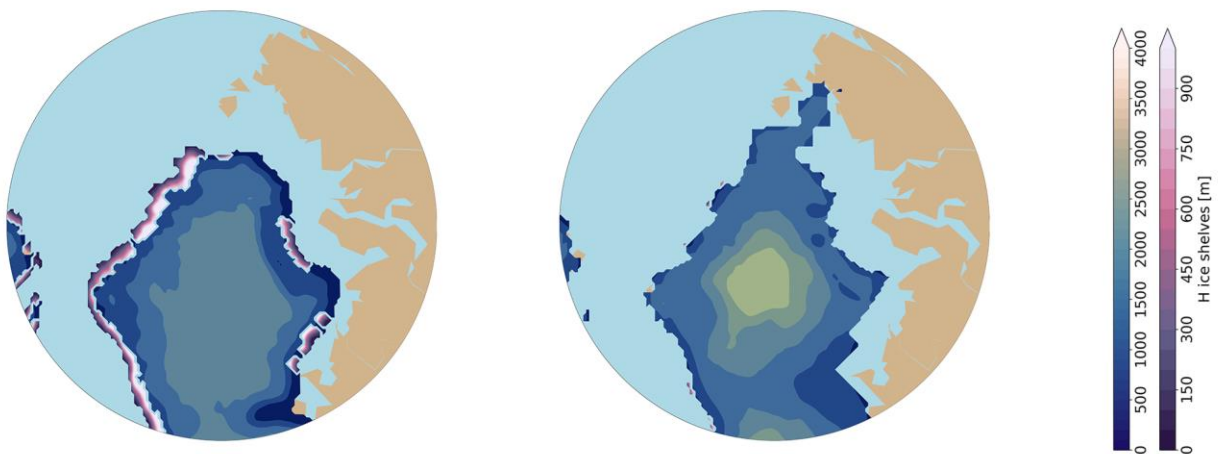


45 **Figure S2:** up: Ice volume simulated at the end of the 100.000 years of spin up simulations for different
 46 values of β_{min} compared to reconstructions. down: same as up but for ice extent.



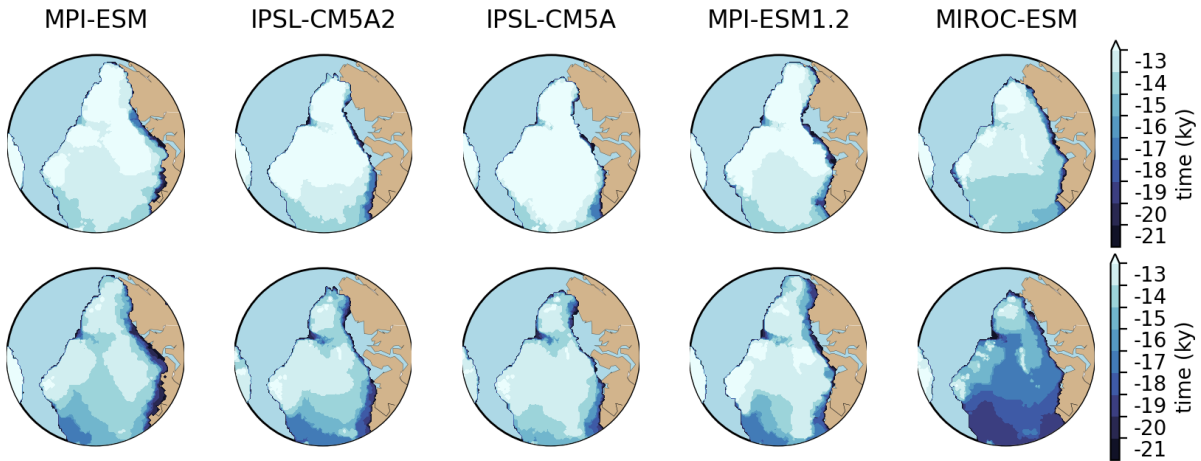
49 **Figure S3:** Initial ice thickness, in meter, of grounded ice (in blue) and ice shelves (in pink) for different
 50 values of β_{min} . The white line shows the DATED1 ice extent at the LGM.
 51

52
 53

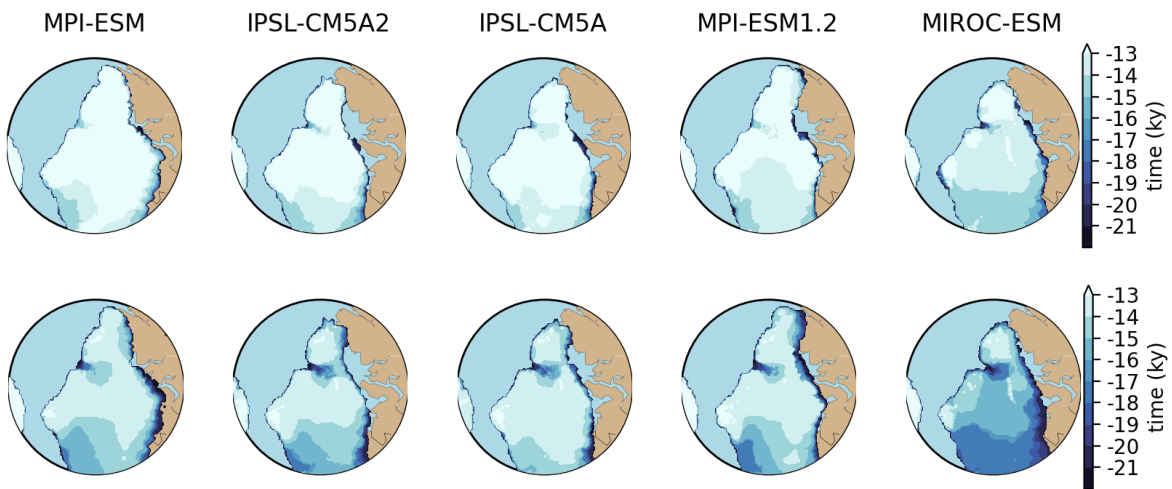


54 **Figure S4:** Ice thickness, in meter, of grounded ice (in blue) and ice shelves (in pink) at the LGM for GLAC1D
 55 (left) and ICE_6G (right) reconstructions
 56

57
 58

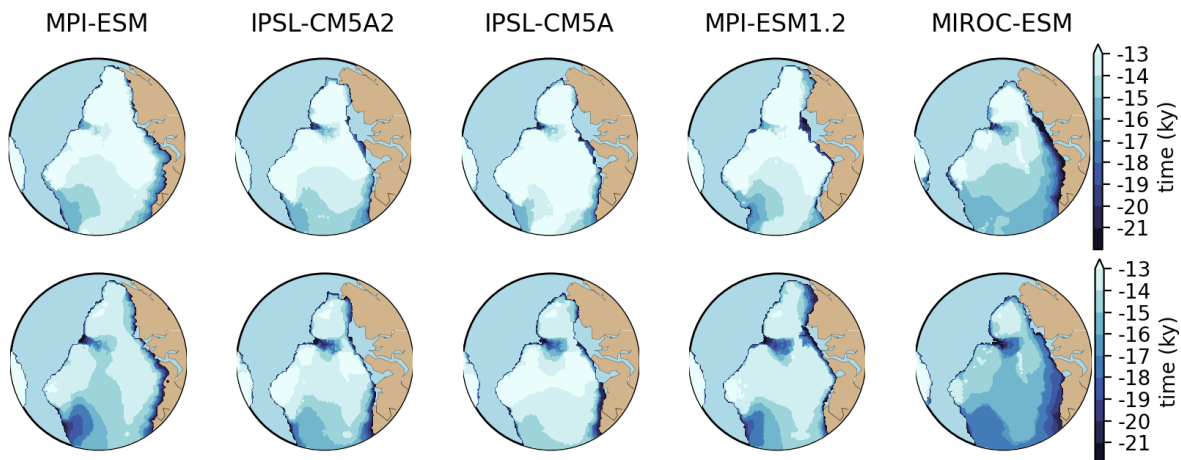


59
 60 **FigureS5:** Date at which deglaciation is completed for each of the GRISLI reference simulations ($\beta_{min} =$
 61 $10 \text{ Pa}\cdot\text{s}\cdot\text{m}^{-1}$) forced by the five PMIP3/PMIP4 models and using the two climate indexes calculated from
 62 the TRACE21k (top) and iLOVECLIM (bottom) simulations.



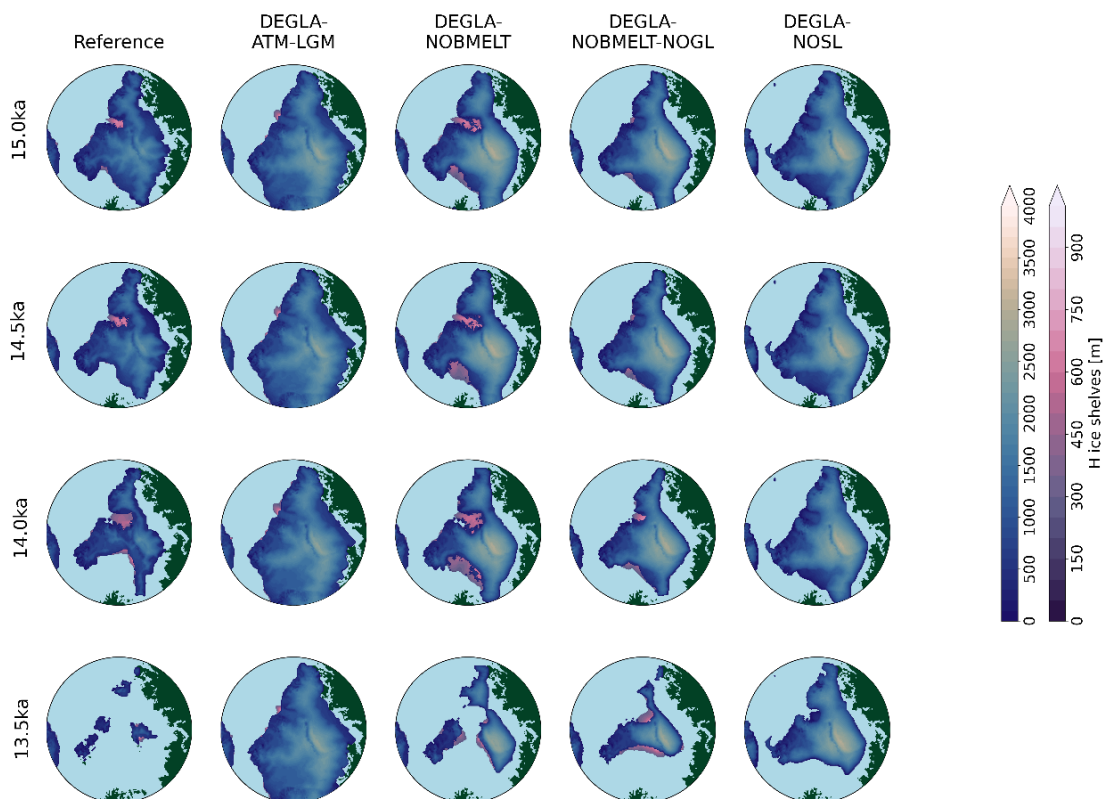
64
 65 **FigureS6:** Same as figure S5 but for $\beta_{min} = 50 \text{ Pa s m}^{-1}$.

66
 67
 68
 69
 70
 71



72
73
74
75
76
77
78

Figure S7: Same as figure S5 but for $\beta_{min} = 100 \text{ Pa s m}^{-1}$.

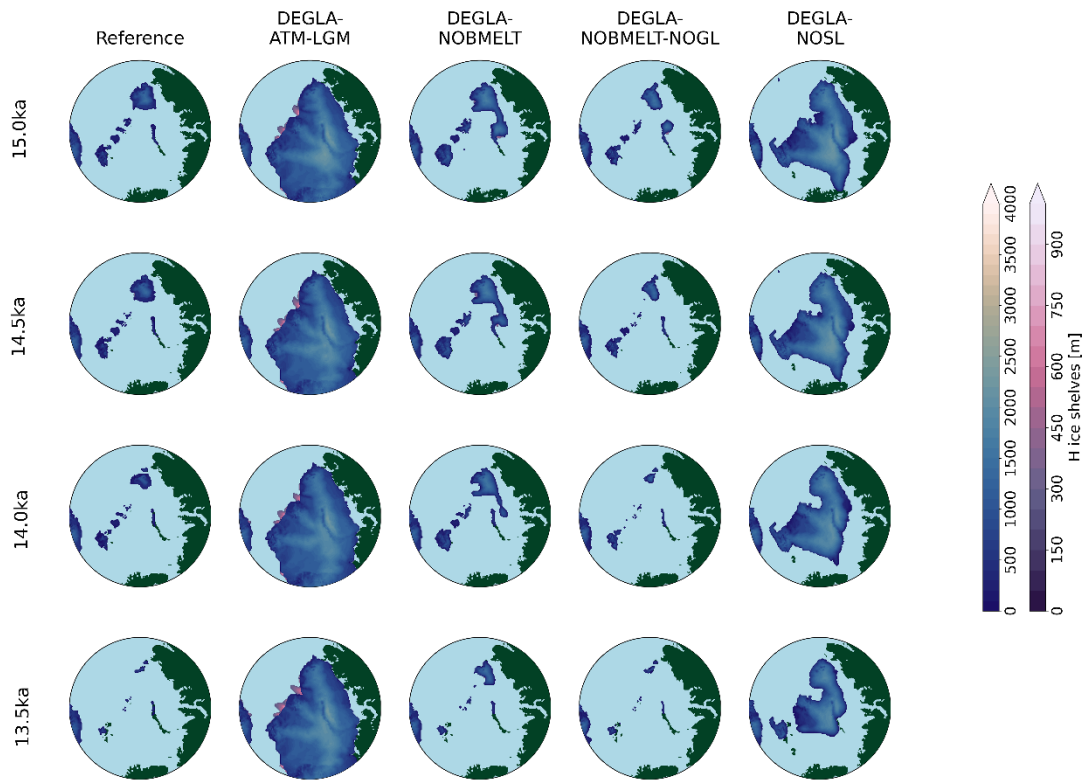


79

80 **Figure S8:** Ice thickness (in meters) of grounded ice (blue shaded areas) and ice shelves (pink shaded
81 areas) at different time steps using the iLOVECLIM index, the MPI-ESM forcing and $\beta_{min} = 10 \text{ Pa.s.m}^{-1}$ for

82 the reference (a), b: the DEGLA-ATM-LGM; c: DEGLA-NOBMELT; d: DEGLA-NOBMELT-NOGL and e: DEGLA-
83 NOSL.

84
85

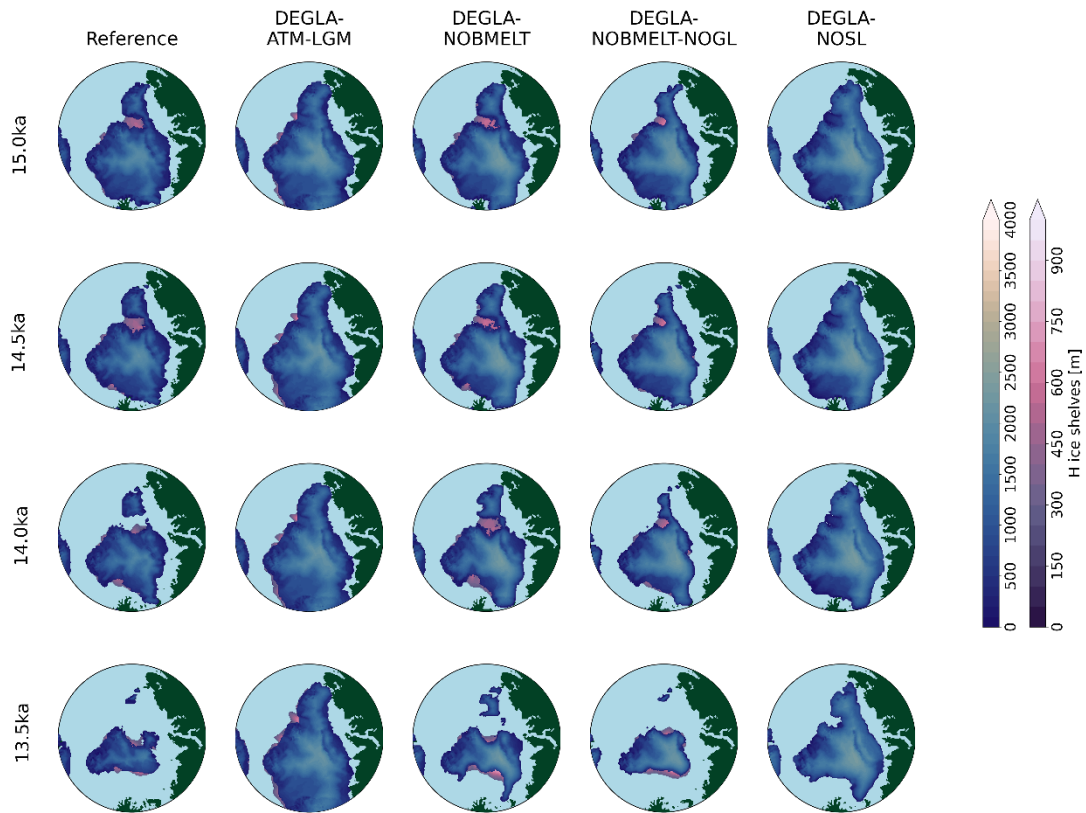


86

87 **Figure S9:** same as Figure S8 but for simulations forced by MIROC

88

89

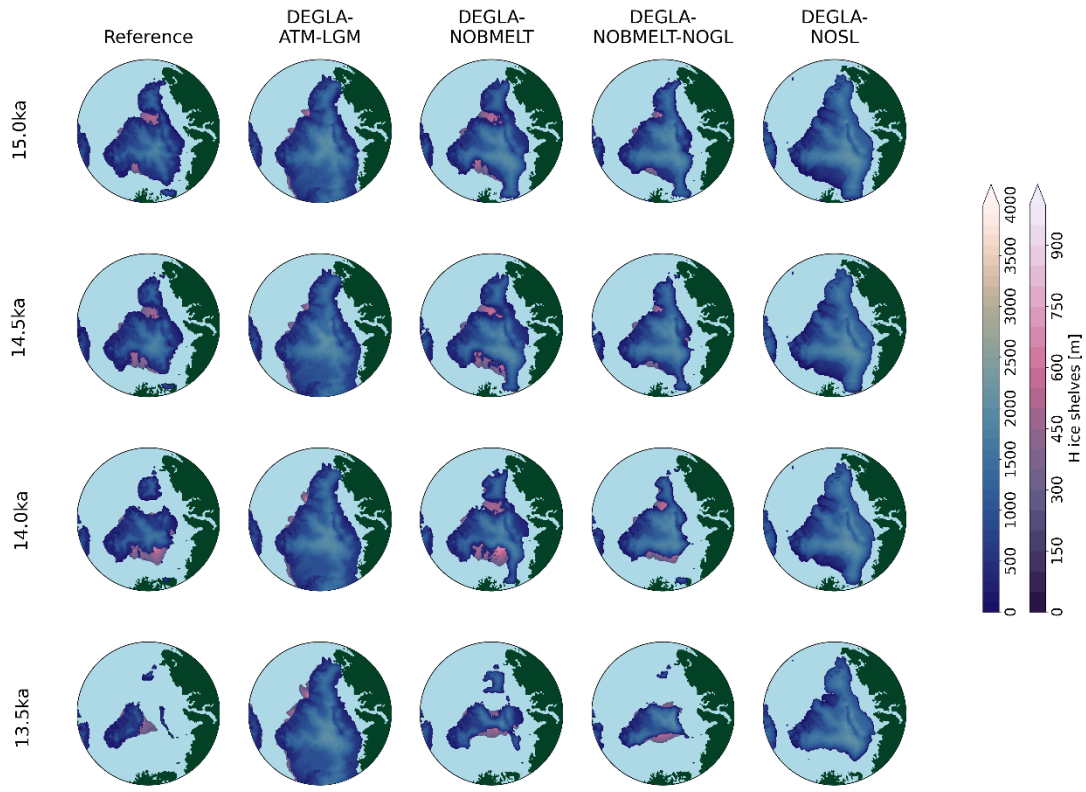


90

91 **Figure S10:** same as Figure S8 but for simulations forced by IPSLCM5LR

92

93



94

95 **Figure S11:** same as Figure S8 but for simulations forced by IPSLCM5A2

96

97

98

99

100

101

102

103

104

105

106

107

108

109

110

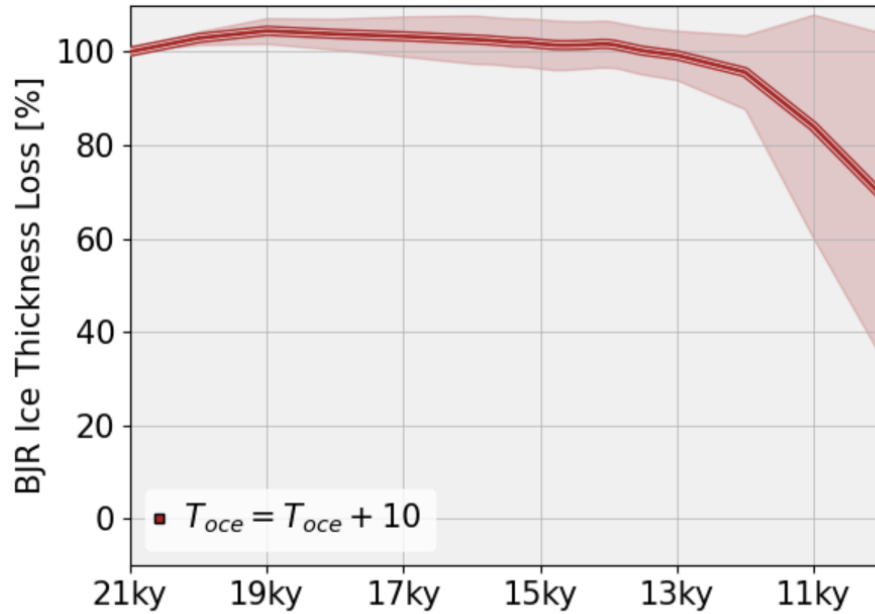
111

112

113

114

115 To highlight the limited role of ocean warming, a new set of experiments was conducted (DEGLA-
116 ATM-LGM-+10C). As in DEGLA-ATM-LGM, atmospheric temperatures were kept fixed at their
117 LGM values. In this experiment, 3D ocean temperatures were artificially increased by +10°C
118 relative to their LGM values. This increase was applied on top of the temporal evolution
119 prescribed by the climate index. Figure S12 shows that, even under these conditions, no
120 significant retreat of the BKIS ice sheet is simulated.



121 **Figure S12:** Multi-model mean of ice thickness loss in the Bjornoyrenna (BJR) region relative to the LGM
122 ice sheet for the $T_{ocean}+10$ experiment, using the iLOVECLIM index. Values of 0% indicate complete ice
123 loss. The y-axis represents ice volume loss relative to the initial ice volume.
124

125
126
127
128
129
130
131
132
133
134
135

136

137 **2. Tables**138 **Table S1:** Model parameters of the GRISLI ice-sheet model used in this study

Parameters	Identifier name	Value
Enhancement factor (SIA)	E_{SIA}	5
Enhancement factor (SSA)	E_{SSA}	0.625
Atmospheric temperature lapse rate	λ	$7 \text{ }^\circ\text{C km}^{-1}$
Precipitation ratio to temperature change	ω	$0.11 \text{ }^\circ\text{C}^{-1}$
Oceanic heat transfer factor	K_t	$7 \text{ m yr}^{-1} \text{ }^\circ\text{C}^{-1}$
Thickness threshold for the calving criterion	H_{cut}	250 m
Relaxation time of the asthenosphere	R_{time}	3000 years
Basal drag parameter	C_f	$1.5 \text{ } 10^{-6} \text{ m yr}^{-1}$

139

140 **Table S2:** Parameterisations of the GRISLI ice-sheet model used in this study

Parameterisations	References
Positive degree-days	Tarasov and Peltier (2002)
Basal melting below ice shelves	Deconto and Pollard (2012)
Flux at the grounding line	Tsai et al. (2015)
Basal friction law	Budd law / Brondex et al. (2017)

141

142

143 **Table S3:** PMIP3 and PMIP4 models used to force GRISLI. The fourth column indicates the choice of the ice sheet
144 boundary condition at the LGM for each GCM simulation.

model	References	PMIP/CMIP	Boundary condition
MPI-ESM-P	Adloff et al. (2018)	CMIP5 PMIP3	PMIP3 ice sheet
MIROC-ESM	Sueyoshi et al. (2013)	CMIP5 PMIP3	PMIP3 ice sheet
IPSL-CM5A-LR	Dufresne et al. (2013)	CMIP5 PMIP3	PMIP3 ice sheet
IPSL-CM5A2	Sepulchre et al. (2020)	CMIP6 PMIP4	ICE-6G_C
MPI-ESM1.2	Mauritsen et al. (2019)	CMIP6 PMIP4	ICE-6G_C

145

146 **Table S4:** List of the different reference deglaciation experiments conducted with the GRISLI ice sheet
 147 model: Experiment names (1st column), climate forcing (2nd column), climate index used to establish an
 148 evolving climatology and force GRISLI between the LGM and the pre-industrial period (3rd column) and
 149 β_{min} value (4th column).

Experiment names	Climate forcing	Climate index	β_{min}
DEGLA-MPI-iLOVECLIM-10	MPI-ESM-P	iLOVECLIM	10
DEGLA-MPI-TRACE21k-10	MPI-ESM-P	TRACE21k	10
DEGLA-MPI1.2-iLOVECLIM-10	MPI-ESM1.2	iLOVECLIM	10
DEGLA-MPI1.2-TRACE21k-10	MPI-ESM1.2	TRACE21k	10
DEGLA-MIROC-iLOVECLIM-10	MIROC-ESM	iLOVECLIM	10
DEGLA-MIROC-TRACE21k-10	MIROC-ESM	TRACE21k	10
DEGLA-IPSLCM5LR-iLOVECLIM-10	IPSL-CM5A-LR	iLOVECLIM	10
DEGLA-IPSLCM5LR-TRACE21k-10	IPSL-CM5A-LR	TRACE21k	10
DEGLA-IPSLCM5A2-iLOVECLIM-10	IPSL-CM5A2	iLOVECLIM	10
DEGLA-IPSLCM5A2-TRACE21k-10	IPSL-CM5A2	TRACE21k	10

150

Experiment names	Climate forcing	Climate index	β_{min}
DEGLA-MPI-iLOVECLIM-50	MPI-ESM-P	iLOVECLIM	50
DEGLA-MPI-TRACE21k-50	MPI-ESM-P	TRACE21k	50
DEGLA-MPI1.2-iLOVECLIM-50	MPI-ESM1.2	iLOVECLIM	50
DEGLA-MPI1.2-TRACE21k-50	MPI-ESM1.2	TRACE21k	50
DEGLA-MIROC-iLOVECLIM-50	MIROC-ESM	iLOVECLIM	50
DEGLA-MIROC-TRACE21k-50	MIROC-ESM	TRACE21k	50
DEGLA-IPSLCM5LR-iLOVECLIM-50	IPSL-CM5A-LR	iLOVECLIM	50
DEGLA-IPSLCM5LR-TRACE21k-50	IPSL-CM5A-LR	TRACE21k	50
DEGLA-IPSLCM5A2-iLOVECLIM-50	IPSL-CM5A2	iLOVECLIM	50
DEGLA-IPSLCM5A2-TRACE21k-50	IPSL-CM5A2	TRACE21k	50

151

Experiment names	Climate forcing	Climate index	β_{min}
DEGLA-MPI-iLOVECLIM-100	MPI-ESM-P	iLOVECLIM	100
DEGLA-MPI-TRACE21k-100	MPI-ESM-P	TRACE21k	100
DEGLA-MPI1.2-iLOVECLIM-100	MPI-ESM1.2	iLOVECLIM	100
DEGLA-MPI1.2-TRACE21k-100	MPI-ESM1.2	TRACE21k	100
DEGLA-MIROC-iLOVECLIM-100	MIROC-ESM	iLOVECLIM	100
DEGLA-MIROC-TRACE21k-100	MIROC-ESM	TRACE21k	100
DEGLA-IPSLCM5LR-iLOVECLIM-100	IPSL-CM5A-LR	iLOVECLIM	100
DEGLA-IPSLCM5LR-TRACE21k-100	IPSL-CM5A-LR	TRACE21k	100
DEGLA-IPSLCM5A2-iLOVECLIM-100	IPSL-CM5A2	iLOVECLIM	100
DEGLA-IPSLCM5A2-TRACE21k-100	IPSL-CM5A2	TRACE21k	100

152